AIMS Materials Science, 6(5): 798–805.
DOI: 10.3934/matersci.2019.5.798
Received: 11 June 2019
Accepted: 18 July 2019
Published: 02 September 2019

http://www.aimspress.com/journal/Materials

Research article

Evaluation of tensile properties of ferrite single-phase low-carbon steel with different initial microstructures

Toshio Ogawa[1,*], Hiroyuki Dannoshita[2] and Yoshitaka Adachi[1]

[1] Department of Materials Design Innovation Engineering, Graduate School of Engineering, Nagoya University, Furo-cho, Chikusa-ku, Nagoya, Aichi 464-8603, Japan
[2] Department of Mechanical Engineering, Materials Science, and Ocean Engineering, Graduate School of Engineering Science, Yokohama National University, 79-1 Tokiwadai, Hodogaya-ku, Yokohama, Kanagawa 240-8501, Japan

* **Correspondence:** Email: ogawa.toshio@material.nagoya-u.ac.jp; Tel: +81527893579; Fax: +81527894858.

Abstract: The tensile properties of ferrite single-phase low-carbon steel with different initial microstructures were evaluated. Three types of hot-rolled sheet specimens with different microstructures—specimen P (consisting of ferrite and pearlite), specimen B (consisting of bainitic structures), and specimen M (consisting of fully martensitic structures) were used. After hot rolling, these specimens were cold-rolled, subsequently heated to the finishing temperature of ferrite recrystallization, and then water-quenched to room temperature. The recrystallized ferrite grain size decreased in the specimen order of B > P > M. The distribution of cementite was comparatively homogeneous in specimens B and M, whereas that in specimen P was heterogeneous. The yield and tensile strengths decreased in the specimen order of M > P > B. Calculations using the Hall–Petch equation revealed that the yield strength of each specimen depended mainly on the recrystallized ferrite grain size. The total elongation decreased in the specimen order of B > P > M, whereas the local elongation was approximately the same in all of the specimens. In addition, the number of dimples decreased in the specimen order of M > B > P, whereas the size of dimples decreased in the specimen order of P > B > M. These results suggest that the homogeneous distribution of cementite and the fine recrystallized ferrite grains in specimen M suppress void coalescence, thereby resulting in a good balance between the tensile strength and the local elongation.

Keywords: low-carbon steel; cementite; recrystallization; initial microstructure; tensile property

1. Introduction

The automobile industry strongly demands low-carbon high-strength steel, and the tensile strength of steel continues to increase. Various high-strength steels have been developed to meet this demand. Dual-phase (DP) and transformation-induced plasticity (TRIP) steels are typical high-strength steels with excellent ductility [1–4]. However, the formabilities (e.g., bendability and hole-expandability) of these steels are inferior compared to single-phase steels, which is a serious problem such as a cracking during press forming [5,6]. Thus, steels with a good combination of ductility and formability are needed.

For DP steels, the effect of martensite distribution on tensile properties has been investigated by several authors [7–10]. For instance, Tomota et al. [7] have demonstrated that connected martensite in DP steels leaded to an increase in tensile strength and in the strain-hardening exponent. In addition, a decrease in the diameter of the dispersed martensite has been reported to improve the balance between strength and local elongation [9].

Methods of improving the formability of high-strength steels have been proposed in previous studies [5,6]. For instance, a homogeneous microstructure of the steels enhances their formability [5]. The homogeneous microstructure means equiaxed grains, a homogeneous distribution of hard phases and precipitates, and decomposition of the layered microstructure. In the case of low-carbon steel, we have previously demonstrated that the morphology of recrystallized ferrite grains and the distribution of martensite were both strongly dependent on the initial microstructures before annealing [11,12]. In particular, recrystallized ferrite grains are equiaxed and the distribution of martensite is homogeneous after annealing when the initial microstructure includes martensite. Therefore, we have suggested that properly controlling the initial microstructures before annealing was important for improving the formability of low-carbon steels. However, the effect of initial microstructures on the tensile properties of low-carbon steels has not been investigated yet. Achieving a good combination of ductility and formability requires knowledge of the effect of low-carbon steels' initial microstructures on their tensile properties.

Thus, the purpose of the present study is to evaluate the tensile properties of a low-carbon steel and correlate these properties with the steels' initial microstructure. This work is a fundamental study on the tensile properties of the ferrite phase. All of the tests were performed with ferrite single-region annealing.

2. Materials and method

The chemical composition of the tested steel (in mass%), which was the same as used in our previous studies [11,12] was 0.1C–2.0Mn. The vacuum-melted ingots (approximately 100 mm in thickness) were rough rolled to a thickness of 30 mm. The rough-rolled steels were hot-rolled at a finishing temperature of 900 °C, which corresponds to the austenite region, to a thickness of 3.0 mm, and subsequently water cooled to 650 °C (specimen P), 500 °C (specimen B), or less than 100 °C (specimen M) by water jet. All specimens were subsequently cooled to room temperature in air. The temperature during cooling was evaluated via measurement of the surface temperature. Specimen P consisted of ferrite and pearlite. Specimen B consisted of bainitic structures, and specimen M consisted of fully martensitic structures. The hot-rolled sheets were cold-rolled to a thickness of 1.0 mm (reduction 67%) in a four-high cold rolling mill at a rolling speed of 15 m/min. The

microstructures of the hot-rolled and cold-rolled sheets have been reported for each specimen in our previous article [11].

After cold-rolling, the specimens were heated to each finishing temperature of ferrite recrystallization at a rate of 0.5 °C/s using an electric furnace, and then water-quenched to room temperature within 2 s after the removal of specimens from the furnace. The finishing temperature of the ferrite recrystallization in specimens P, B, and M was 650, 660, and 610 °C, respectively [11].

The microstructures of nital-etched specimens (etching time approximately 10 s) were observed by scanning electron microscopy (SEM) at an accelerating voltage of 5 kV. Nital etchant has been widely used in the metallography of steels and it was suitable for observing the microstructures in the present study. Tensile test of the specimens was conducted at room temperature and at a strain rate of 1.67×10^{-3} s^{-1}. The JIS Z 2201 standard for the tensile test specimens was used. Standard deviations of the tensile properties were calculated from the results obtained from two specimens. The fracture surfaces of the specimens were observed by SEM. The number and size of dimples in the fracture surfaces were quantified using the image-analysis program ImageJ. The SEM images of fracture surfaces were subjected to binarization processing using ImageJ, and the number of dimples (black region) was estimated. The morphology of dimples was assumed to be oval for purpose of analysis using ImageJ, and the average value of the major and minor axes of the oval dimples was defined as the size of the dimples. Void observations were conducted at distance of approximately 3000 μm from the fractured surface by SEM. The number of void was estimated using twenty SEM images with a total area of approximately 3200 μm^2 in each specimen.

3. Results and discussion

Figure 1 shows the microstructures of the specimens immediately after completion of ferrite recrystallization. The recrystallized ferrite grain size decreased in the specimen order of B > P > M. Furthermore, the recrystallized ferrite grains in specimen M were finer and more equiaxed than those in specimens P and B. The distribution of cementite was comparatively homogeneous in specimens B and M, whereas it was heterogeneous in specimen P.

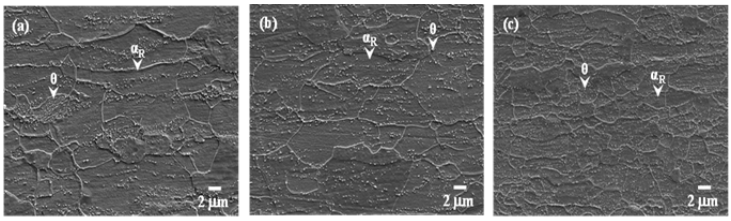

Figure 1. Microstructures of specimens P (a), B (b), and M (c) immediately after completion of ferrite recrystallization. α_R: recrystallized ferrite; θ: cementite particles.

The yield and tensile strengths of the specimens are shown in Figure 2a. The yield and tensile strengths decreased in the specimen order of M > P > B. The local and total elongations of the specimens are shown in Figure 2b. Notably, the total elongation decreased in the specimen order of B > P > M whereas the local elongation was approximately the same in all of the specimens. Here, we focus on the relationship between the recrystallized ferrite grain size of the specimens and their

yield strength. According to the Hall–Petch equation [13,14], a smaller grain size resulted in an increase of yield strength. The Hall–Petch equation is expressed as:

$$\sigma = \sigma_0 + kd^{-1/2}$$

where σ is the yield strength; σ_0 is the friction stress; k is a material-specific constant, and d is the average grain size. We have reported that the recrystallized ferrite grain size of specimens P, B, and M was 4.6, 5.2, and 3.3 μm, respectively [11]. Moreover, in the case of low-carbon steel, Takaki et al. [15] have proposed estimated values of 100 and 600 for σ_o and k in the Hall–Petch equation, respectively. Therefore, the yield strength of all specimens can be estimated using the Hall–Petch equation. Figure 3 shows the relationship between the yield strength obtained by tensile test and that calculated using the Hall–Petch equation. The yield strength obtained by tensile test is in good agreement with that calculated using the Hall–Petch equation. Thus, the yield strength of each specimen is mainly dependent on the recrystallized ferrite grain size.

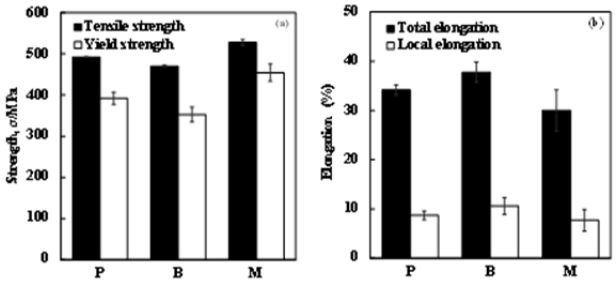

Figure 2. The yield and tensile strengths (a) and the local and total elongations of the specimens (b).

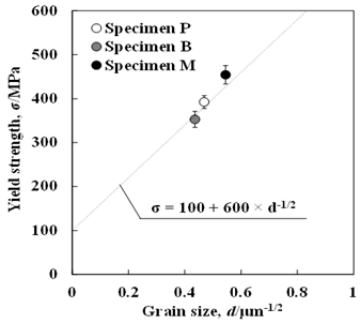

Figure 3. Relationship between the yield strength obtained by tensile test and that calculated using the Hall–Petch equation.

For the dominant factor of yield strength, precipitation strengthening by cementite should be considered. A smaller precipitate size is known to lead to a greater degree of precipitation strengthening. We have previously demonstrated that the spheroidal cementite in specimen M was finer than that in specimens P and B [11]. This observation indicates that the degree of cementite precipitation strengthening in specimen M is greater than that in specimens P and B. In the case of specimen M, the yield strength obtained by tensile test was slightly larger than that calculated using the Hall–Petch equation (Figure 3). Therefore, the difference between the yield strength of specimen

M obtained by tensile test and that calculated using the Hall–Petch equation is attributable to the precipitation strengthening of cementite.

In general, the greater the strength of a material, the lower its elongation. As shown in Figure 2, the tensile strength and the total elongation of each specimen also exhibit a trade-off relationship in the present study. Notably, the local elongation was approximately the same in all of the observed specimens. This result implies that specimen M has a good balance between tensile strength and local elongation. The local elongation of metals has been reported to be dependent on the nucleation, growth, and coalescence of voids [16]. Therefore, we discussed void nucleation and coalescence on the basis of the features of dimples in the fracture surfaces. Figure 4 shows SEM micrographs of the fracture surfaces of the specimens. The fracture surface of all specimens was ductile and consisted of multiple dimples; the dimple size in all specimens varied. The average number and size of the dimples in the specimens are shown in Figure 5. The number of dimples decreased in the specimen order of M > B > P (Figure 5a), whereas the size of dimples decreased in the specimen order of P > B > M (Figure 5b).

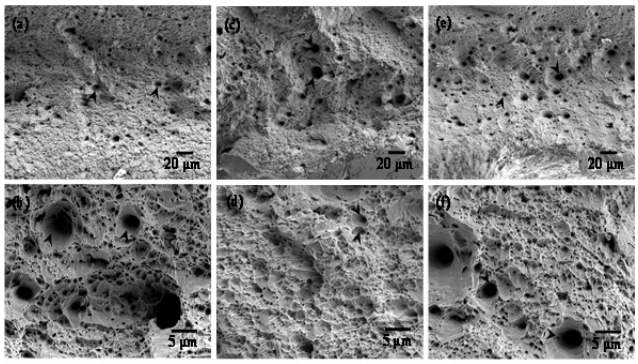

Figure 4. SEM micrographs of fracture surfaces of the specimens P (a, b), B (c, d), and M (e, f). Black arrows: dimples.

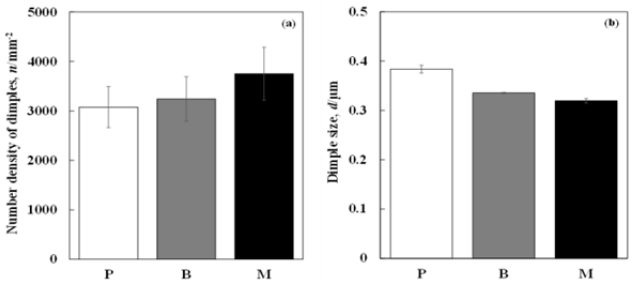

Figure 5. Average number (a) and size (b) of dimples in the specimens.

With respect of void nucleation, voids have been demonstrated to generally nucleate at hard phases and inclusions [17–19]. As shown in Figure 6, the voids mainly nucleated at cementite in all specimens. Therefore, the void nucleation sites in specimens B and M are likely distributed homogeneously because the distribution of cementite in these specimens was comparatively homogeneous (Figure 1b,c). In contrast, the void nucleation sites in specimen P should be localized because the distribution of cementite was heterogeneous (Figure 1a). These results suggest that the

number of void nucleation sites at cementite in specimens B and M is larger than that in specimen P. Moreover, the voids in interstitial-free (IF) steels mainly nucleate at ferrite/ferrite interfaces (i.e., ferrite grain boundaries) [16]. As shown in Figure 1, the recrystallized ferrite grain size decreased in the specimen order of B > P > M. Thus, the number of void nucleation sites at ferrite grain boundaries in specimens M is likely larger than that in specimens P and B. As shown in Figure 6, the number of void nucleation sites at ferrite grain boundaries in specimen M was larger than that in specimens P and B. From the viewpoint of the void nucleation sites at cementite and ferrite grain boundaries, specimen M likely contains the most void nucleation sites. In addition, the number of dimples in specimen M is apparently larger than that in specimens P and B because the number of the void nucleation sites in specimen M is larger than that in specimens P and B.

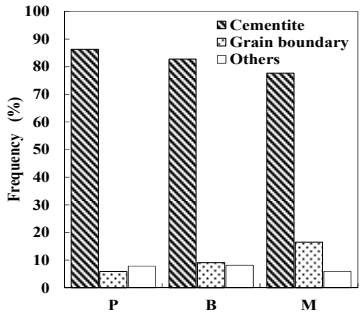

Figure 6. The number of void at each nucleation site.

Void coalescence has been speculated to depend on the distribution of cementite [19]. Furthermore, Furukimi et al. [20] have revealed that voids nucleate at Cr precipitates in Cr-added steels and that the local elongation increases with increasing mean interparticle spacing of Cr precipitates. These previous studies imply that void coalescence easily occurs when the spacing among the void nucleation sites is small. Therefore, the size of dimples in specimen P is likely larger than that in specimens B and M because the distribution of cementite is heterogeneous and the spacing of cementite is small in specimen P. As shown in Figure 7, the voids nucleated at cementite spherodized in pearlite colonies of specimen P. In addition, void coalescence has been demonstrated to be difficult when the distribution of the void nucleation sites is homogeneous [9]. Accordingly, the size of dimples in specimen M is smaller than that in specimen B because the number of void nucleation sites in specimen M is large and the distribution of the voids is homogeneous.

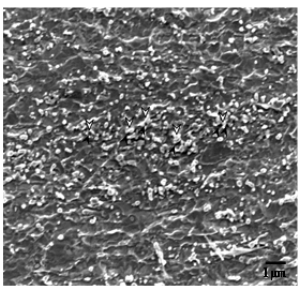

Figure 7. SEM micrograph of voids of the specimen P. White arrows: cementite particles; black arrows: voids.

High local elongation can be obtained by suppressing the growth and coalescence of voids [20]. As previously mentioned, the void coalescence in specimen M was suppressed the most, whereas that was accelerated the most in specimen P. These results indicate that the local elongation of specimen M, which has high tensile strength increases, whereas that of specimen P, which exhibits low tensile strength decreases. Thus, we concluded that the local elongation of each specimen can be explained on the basis of the features (number and size) of dimples.

4. Conclusions

The tensile properties of ferrite single-phase low-carbon steel with different initial microstructures were evaluated, and the following results were obtained:

(1) The yield and tensile strengths decreased in the specimen order of M > P > B. As a result of calculations using the Hall–Petch equation, the yield strength of each specimen was mainly dependent on the recrystallized ferrite grain size.

(2) The total elongation decreased in the specimen order of B > P > M, whereas the local elongation was approximately the same in all of the specimens.

(3) The number of dimples decreased in the specimen order of M > B > P, whereas the size of dimples decreased in the specimen order of P > B > M. The local elongation of each specimen was explained on the basis of the features (number and size) of its dimples.

Acknowledgments

This work was supported by a research grant from the Hitachi Metals Materials Science Foundation, Japan.

Conflict of interests

All authors declare that there is no conflict of interest.

References

1. Maki T, Onodera H, Tamura I (1975) Trip phenomenon in residual austenite of Fe–Ni–C alloy. *J Soc Mater Sc*i 24: 150–155.
2. Matsumura O, Sakuma Y, Takechi H (1987) Enhancement of elongation by retained austenite in intercritical annealed 0.4C–1.5Si–0.8Mn steel. *Trans ISIJ* 27: 570–579.
3. Murata M, Kobayashi J, Sugimoto K (2010) Stretch-flangeability of ultra high-strength low alloy TRIP-aided sheet steels with mixed structure matrix of bainitic ferrite and martensite. *Tetsu-to-Hagane* 96: 84–92.
4. Moor ED, Speer JG, Matlock DK, et al. (2011) Effect of carbon and manganese on the quenching and partitioning response of CMnSi steels. *ISIJ Inter* 51: 137–144.
5. Nonaka T, Fujita N, Taniguchi Y, et al. (2007) Development of ultra-high-strength steel sheets with excellent formabilities. *Materia Jpn* 46: 108–110.
6. Takahashi M (2002) High strength steel sheets for light weight auto-bodies. *Bull Iron Steel Inst Jpn* 7: 870–877.

7. Tomota Y, Tanimoto I, Kuroki K (1982) On the deformation behavior of ferrite-martensite: two-ductile-phase steels. *T Jpn Soc Mech Eng A* 48: 528–536.
8. Sugimoto K, Sakaki T, Fukusato T, et al. (1985) Influence of martensite morphology on initial yielding and strain hardening in a 0.11–1.36Mn dual-phase steel. *Tetsu-to-Hagane* 71: 994–1001.
9. Kondo D, Kunishige K, Ueji R (2006) Effects of the grain size and volume fraction of second hard phase on mechanical properties of dual phase steel. *Tetsu-to-Hagane* 92: 457–463.
10. Jiang Z, Guan Z, Lian J (1995) Effects of microstructural variables on the deformation behaviour of dual-phase steel. *Mater Sci Eng A-Struct* 190: 55–64.
11. Ogawa T, Dannoshita H, Maruoka K, et al. (2017) Microstructural evolution during cold rolling and subsequent annealing in low-carbon steel with different initial microstructures. *J Mater Eng Perform* 26: 3821–3830.
12. Dannoshita H, Ogawa T, Maruoka K, et al. (2019) Effect of initial microstructures on austenite formation behavior during intercritical annealing in low-carbon steel. *Mater Trans* 60: 165–168.
13. Hall EO (1951) The deformation and ageing of mild steel: III discussion of results. *Proc Phys Soc B* 64: 747–753.
14. Petch NJ (1953) The orientation relationships between cementite and α-iron. *J Iron Steel Inst* 174: 25–28.
15. Takaki S, Kawasaki K, Kimura Y (2001) Mechanical properties of ultra fine grained steels. *J Mater Process Tech* 117: 359–363.
16. Furukimi O, Takeda Y, Yamamoto M, et al. (2017) Voids nucleation and growth examination during tensile deformation for IF steel by synchrotron X-ray laminography and EBSD. *Tetsu-to-Hagane* 103: 475–482.
17. Tohgo K, Ishii H, Hiramatsu K, et al. (1993) Influence of cementite volume fraction on mechanical properties and fracture toughness in spheroidized cementite steel: study on fracture behavior of particulate-reinforced composite. *T Jpn Soc Mech Eng A* 59: 1617–1624.
18. Fujita T, Kariya N, Nakamura N, et al. (2005) Effect of microstructure on elongation in cold-rolled high carbon steel sheets. *Tetsu-to-Hagane* 91: 616–622.
19. Maeda M, Shimamura J, Suzuki S (2017) Void formation by cementite and local misorientation evaluation during tensile deformation in high strength steel sheets. *Tetsu-to-Hagane* 103: 483–490.
20. Furukimi O, Niigaki S, Yamada N, et al. (2013) Local deformation energy and void formation behavior in 16%Cr ferritic steel. *Tetsu-to-Hagane* 99: 60–69.

AIMS Press